technische universität dortmund

Laser-Assisted Magnetic Resonance of Semiconductor Nanostructures

Semiconductor nanostructures are used in many different materials, including semiconductor lasers and other optoelectronic devices. Magnetic resonance is one of the most important techniques for characterizing such structures. However, its limited sensitivity requires specialized techniques that provide sufficiently high sensitivity and selectivity for structures with length scales of the order of nanometers.

Physical Background

Quantum-confined semiconductors

Figure 1 shows a typical example of a semiconductor heterostructure where electrons are confined in quantum wells or quantum dots. The bandgap of the AlGaAs barriers is larger than that of the GaAs wells. The charge carriers are therefore confined in the quantum wells, whose thickness is of the order of a few nm. At low temperatures, this is less than the coherence length of the electrons. As a result, the energy levels of the electrons become discrete. This can be seen, e.g., in the photoluminescence spectrum, where every quantum well emits photons at a specific wavelength: In the thinnest quantum wells, the electronic ground state of the conduction band has the highest energy and the emission wavelength is therefore shifted to shorter wavelengths.

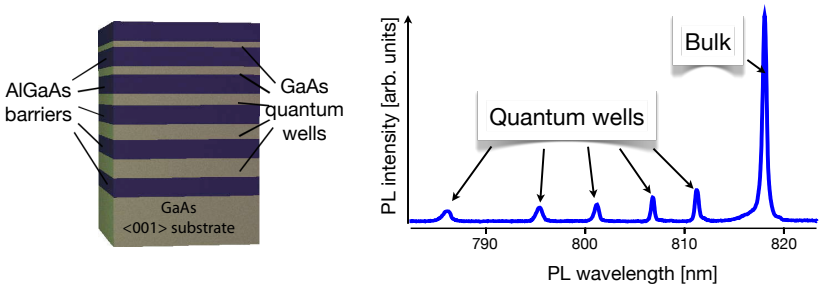

Figure 1: GaAs / AlGaAs multiple-quantum well structure and photoluminescence spectrum.

Optical polarization

In thermal equilibrium, the populations of different angular momentum states are almost identical. This can be changed by optical pumping with resonant polarized light. Fig. 2 shows the principle of optical pumping in a semiconductor quantum well with a p-type valence band and an s-type conduction band. The orbital- and spin-angular momentum combine to a total angular momentum of $J = 1/2$ in the conduction band and $J = 3/2$ in the valence band. The $J = 1/2$ angular momentum states of the valence band are lower in energy (not shown in the figure) and therefore always fully occupied. In the absence of a magnetic field, the four m_j susbstates of the $J = 3/2$ valence band state are degenerate in bulk crystals. However, in a quantum well, where the symmetry of the Hamiltonian is reduced by the confinement potential perpendicularly to the layers, the $m_J = \pm 3/2$ states (known as heavy holes) have a higher energy than the $m_J = \pm 1/2$ states (the light holes). Optical photons close to the band edge of the system therefore couple only to the transitions from the $m_J = \pm 3/2$ valence band states to the $m_J = \pm 1/2$ states of the conduction band. Angular momentum selection rules determine which of the two possible transitions, $|m_J = -3/2\rangle \leftrightarrow |m_{J'} = -1/2\rangle$ or $|m_J = +3/2\rangle \leftrightarrow |m_{J'} = +1/2\rangle$ couples to the radiation field. For circular polarization, the photons therefore create fully spin-polarized electrons in the conduction band and holes in the valence band.

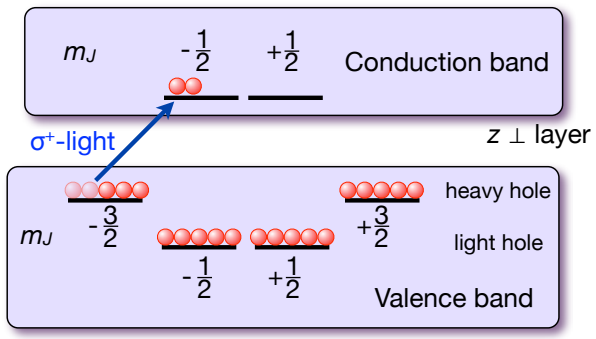

Figure 2: Optical pumping in semiconductor nanostructures with direct band-gap.

Nuclear spins

Most of the isotopes found in semiconductor materials have non-vanishing nuclear spin, e.g. $I = 3/2$ for ^{69}Ga, ^{71}Ga, and ^{75}As. If these nuclear spins are in contact with an unpaired electron, they experience a hyperfine interaction, which can be written as $\mathcal{H}_{hf} = \sum_i A_i \vec{I}_i \cdot \vec{S}$, where A_i quantifies the strength of the interaction between the i-th nuclear spin $\vec{I}_i$ and the electron spin $\vec{S}$. This interaction contains, among others, the so-called flip-flop term $I_+S_- + I_-S_+$, which drives correlated flips of the electronic and nuclear spins. In thermal equilibrium, the polarization of the nuclear spins is vanishingly small, while the optical pumping can generate almost completely polarized electronic spins. The flip-flop processes can therefore transfer polarization from the electronic to the nuclear spins.

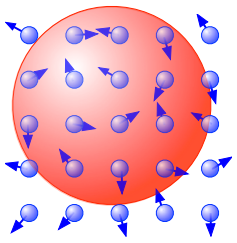

Figure 3: Interaction of an electron with nuclear spins via Fermi contact.

One effect of the nuclear spin polarization is that the large number of nuclear spins that are coupled to the electron spin starts to affect the evolution of the electronic spin. The overall effect is similar to that of a magnetic field and can therefore change the polarization of the luminescence that is emitted when a hole and an electron recombine to emit a photon. The polarization of the emitted photoluminescence is therefore one of the possible measures that allow one to monitor the polarization of the nuclear spins.

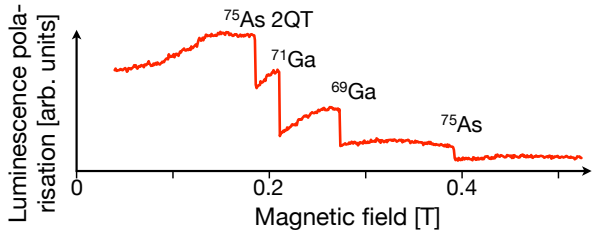

Figure 4: Optically detected nuclear magnetic resonance from a single GaAs quantum well. The system was irradiated with a radio frequency field with $\omega_{rf}/2\pi$= 5 MHz.

If a radio-frequency field is applied to the system, whose frequency fulfills the condition $\omega_{rf} = \omega_L = \gamma B_0$, where ω_{rf} is the frequency of the alternating magnetic field, ω_L is the Larmor frequency of the nuclear spin, γ it's gyromagnetic ratio and B_0 the flux density of the static magnetic field, it can generate transitions between the nuclear spin states. These transitions will typically reduce the nuclear spin polarization, as in the example shown in fig. 4. For this case, an alternating magnetic field with a frequency of ω_{rf}=5 MHz was applied to the sample, which was simultaneously subject to optical pumping with circularly polarized light. As the static magnetic field was increased, several resonance conditions were reached, where the polarization of one of the constituent nuclear spins was saturated by the ac magnetic field. These conditions are marked by the corresponding isotopes. In the case of ^{75}As, the resonance condition is fulfilled for two different fields. At the higher field, just below 0.4 T, transitions occur between states whose magnetic quantum numbers differ by $\Delta m = \pm 1$, in the region below 0.2 T, for $\Delta m = \pm 2$.

Measurement of lattice distortion

If the resonance conditions are analyzed in more detail, they often consist of several steps. Figure 5 shows as an example, the resonance of the ^{75}As nuclei, for the single-quantum ($\Delta m = \pm 1$) transition. In this case, the resonance was measured by keeping the magnetic field constant and scanning the frequency of the applied AC-field. The data clearly show three distinguishable steps of the depolarisation. As shown in the level scheme in the same figure, these three steps can be attributed to the three distinct single quantum transitions that can be induced in an $I = 3/2$ spin. The right-hand panel shows the corresponding NMR spectrum, which consists of a narrow central line, the $-1/2 \leftrightarrow +1/2$ transition and two broader 'satellite transitions' corresponding to the $\pm 3/2 \leftrightarrow \pm 1/2$ transitions.

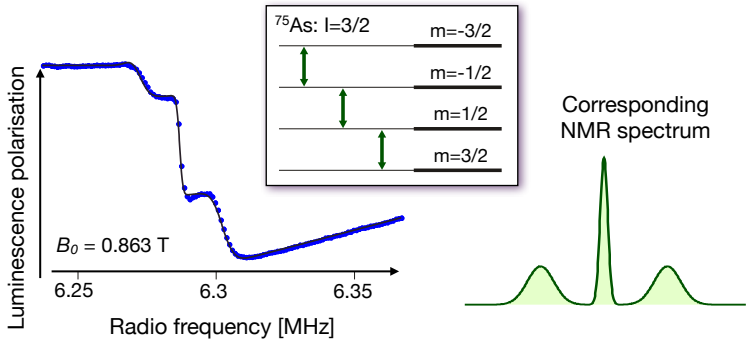

Figure 5: Details of the ^{75}As resonance measured in a constant magnetic field by scanning the RF frequency.

The Zeeman energies for these transitions are the same, but an additional interaction, the nuclear quadrupole coupling $\mathcal{H}_Q = QI_z^2$ shifts these two transitions in opposite direction, as shown in fig. 6. In an ideal crystal, the coupling constant Q vanishes at the positions of the nuclei due to the high site symmetry. This means that all three resonance lines should occur at the same frequency. The experimental data showing three distinct transition frequencies therefore imply that the crystal is deformed in such a way that the environment of the atomic nuclei is slightly asymmetric. It was actually determined, that the degree of asymmetry is a linear function of the splitting between the central line and the satellites [2]. Such deformations occur, e.g., in the vicinity of defects. Since the sensitive volumes, from which spectra are collected, typically contain a very large number of defects, they average over many different line shifts, resulting in a broadening of the satellite lines compared to the central line. This effect is clearly visible in fig. 5. The fact that not only a broadening is visible, but also a splitting, implies that some distortions have correlation lengths larger than the diameter of the sensitive volume, which is determined by the spot size of the laser on the sample (typically of the order of some 10's of μm). Such distortions can arise from strain in the substrate but may also be due to the mounting of the sample.

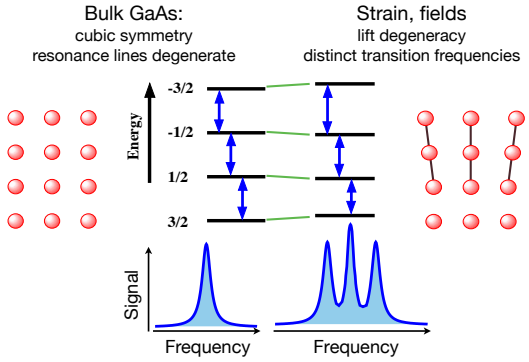

Figure 6: Distortions lower the symmetry. The resulting electric field gradients lift the degeneracy of the NMR transition frequencies.

The strain is in most cases not homogeneous over the sample, but varies with position. Figure 7 shows, as an example, in the left-hand part four measurements taken at four different locations on the same sample. Clearly, the splittings visible in the four spectra show significant variations. The splittings correspond to strain values of up to $6 \cdot 10^{-5}$, as indicated close to the arrows indicating the positions at which the measurements were taken. The right-hand part of the figures shows the distribution of strain over the sample, as evaluated from a large number of similar measurements.

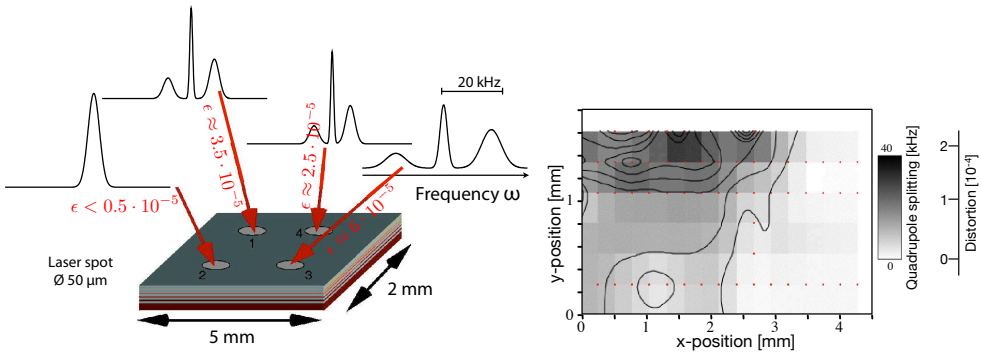

Figure 7: Measurement of lattice distortions at different points on the sample. The left-hand part shows four spectra measured at different positions, indicating different degrees of strain. The right-hand part shows a map of the distortions generated from many measurements at different positions on the sample.

Electric fields

Splittings in NMR spectra occur not only in the presence of lattice distortions, they can also be induced by electric fields that couple to the nuclear quadrupole interaction. Such electric fields may be imposed externally, or they can result from internal charges. In the example shown in fig. 8, the electric field is generated by the Schottky barrier from the contact with a surface electrode [1]. The observed quadrupole splittings increase roughly linearly with depth, which is compatible with a homogeneous space-charge distribution due to the Schottky barrier.

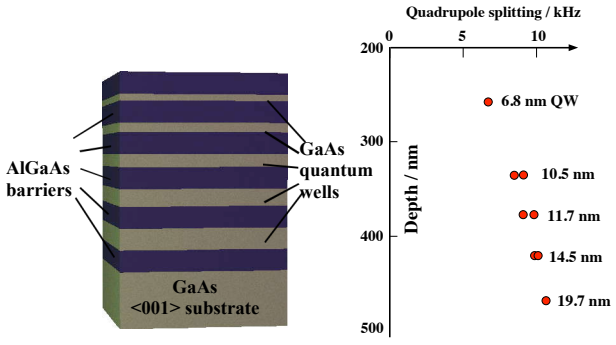

Figure 8: Multiple quantum well with quadrupole splittings measured in different quantum wells.

References

[1] Marcus Eickhoff, Björn Lenzmann, Dieter Suter, Sophia E. Hayes, and Andreas D. Wieck. Mapping of strain and electric fields in GaAs/AlGaAs quantum-well samples by laser-assisted NMR. *Phys. Rev. B*, 67:085308, 2003.

[2] D.J. Guerrier and Richard T. Harley. Calibration of strain vs nuclear quadrupole splitting in III/V quantum wells. *Appl. Phys. Lett.*, 70:1739–1741, 1997.